Mississippi State University
Scholars Junction

Theses and Dissertations | Theses and Dissertations

1-1-2017

# Micromechanical Modeling of the Soil Water Retention Curve using a Coupled Discrete Element-Lattice Boltzmann Method

Jonathan Frank Fili

Follow this and additional works at: https://scholarsjunction.msstate.edu/td

Recommended Citation
Fili, Jonathan Frank, "Micromechanical Modeling of the Soil Water Retention Curve using a Coupled Discrete Element-Lattice Boltzmann Method" (2017). *Theses and Dissertations*. 3090.
https://scholarsjunction.msstate.edu/td/3090

This Graduate Thesis - Open Access is brought to you for free and open access by the Theses and Dissertations at Scholars Junction. It has been accepted for inclusion in Theses and Dissertations by an authorized administrator of Scholars Junction. For more information, please contact scholcomm@msstate.libanswers.com.

# Micromechanical modeling of the soil water retention curve using a coupled discrete element-lattice Boltzmann method

By

Jonathan Frank Fili

A Thesis
Submitted to the Faculty of
Mississippi State University
in Partial Fulfillment of the Requirements
for the Degree of Master of Science
in Civil Engineering
in the Department of Civil and Environmental Engineering

Mississippi State, Mississippi

December 2017

Copyright by

Jonathan Frank Fili

2017

Micromechanical modeling of the soil water retention curve using a coupled discrete element-lattice Boltzmann method

By

Jonathan Frank Fili

Approved:

_____

Farshid Vahedifard
(Major Professor)

_____

John F. Peters
(Committee Member)

_____

John Ramirez Avila
(Committee Member)

_____

James L. Martin
(Graduate Coordinator)

_____

Jason M. Keith
Dean
Bagley College of Engineering

Name: Jonathan Frank Fili

Date of Degree: December 8, 2017

Institution: Mississippi State University

Major Field: Civil Engineering

Major Professor: Dr. Farshid Vahedifard

Title of Study: Micromechanical modeling of the soil water retention curve using a coupled discrete element-lattice Boltzmann method

Pages in Study 41

Candidate for Degree of Master of Science

The Soil Water Retention Curve (SWRC) is a key constitutive relationship describing the behavior of variably saturated soils. The objective of this research is to assess the performance of a hydro-mechanical model, developed by coupling the lattice Boltzmann method (LBM) with the discrete element method (DEM), for micromechanical simulation of the SWRC. The DEM-LBM model is used to examine the effects of wave propagation on fluid-solid interaction. A multi-phase LBM is then employed within a static particle array generated by the DEM to examine the effects of initial fluid density distribution. The SWRCs are generated by recording the liquid pore pressure and the degree of saturation within a porous medium subjected to imbibition for two cases: randomized fluid density simulation (non-unified wetting front) and droplet simulation (unified wetting front). The coupled DEM-multiphase LBM model is shown to be a promising tool to characterize capillary regime in partially saturated porous media.

# DEDICATION

This Thesis work is dedicated to my wife, Dr. Cameron V. Fili. She is the foundation of my life, and her love and support has been paramount to my success.

ACKNOWLEDGEMENTS

I would like to express my deepest gratitude to my advisor, Dr. Farshid Vahedifard. He saw something in me that I did not know that I had and worked with me to make me a better version of myself. He has personally mentored me and taught me what it is to be an engineer. His ability as an advisor and role model is unparalleled, and he is also a wonderful friend. Thank you for all that you have done for me.

I would also like to take a moment to thank Dr. Bohumir Jelinek. Thank you for teaching me to be meticulous in my scientific approach and for developing my skills in High Performance Computing.

I would like to thank Dr. John Peters for his continuous wisdom and sage advice in times of uncertainty.

I give my sincerest thanks to my committee for their guidance and help as I prepare to enter the professional world.

Lastly, I would like to thank my family for their support, especially my sister Christina.

TABLE OF CONTENTS

LIST OF TABLES

LIST OF FIGURES

# CHAPTER I

# INTRODUCTION

## 1.1 Overview

An improved understanding of the mechanics of variably saturated soils and the underlying physics that occur under different degrees of saturation are paramount in geotechnical engineering. The Soil Water Retention Curve (SWRC) is a key constitutive relationship describing the behavior of variably saturated soils. Further insight into this behavior can be gained by studying the role of capillarity on pore adsorption (Lu and Likos, 2004; Fredlund and Rahardio, 1993). The principal experimental approach for geotechnical and groundwater applications is developing the SWRC under inhibition and drainage conditions. The retention curves obtained in such experiments stem from complicated interactions among the air, water and solid phases, details of which are not accessible to direct experimental measurement, despite the progress in modern tomographic imaging technology (Fredlund et. al., 2011; Fredlund et. al., 1996). A variety of approaches have been developed to analyze interactions underlying SWRC (Lu 2016). Numerical simulations offer an effective supplement to physical experiments whereby the detailed interactions among phases can be quantified.

The motivation for this study is to develop a micromechanical model that accurately captures the multi-physical processes in unsaturated soils. Such a model would

enable others in the field to study a wide variety of problems at both the micro-and macro-scale. Such problems could include SWRC experiments, static liquefaction, and cyclic loading on unsaturated soil beds.

## 1.2 Objectives

The main objective of this work is to assess the performance of a novel hydromechanical model, developed by coupling multi-phase Lattice-Boltzmann Method (LBM) with the Discrete Element Method (DEM), for simulating the mechanics of imbibition, beginning with the benchmark validation of the SWRC. A model using a coupled DEM-LBM is used to examine the effect of wave propagation in the single-phase LBM on the fluid-solid interaction. A multi-phase LBM model is then developed to perform a similar study on the effect of initial fluid density distribution on the SWRC.

The performance of the LBM can be a function of several parameters including, but not limited to, both the initial shape of the wetting front and density distributions, as well as the waves propagating through the system-both physical and artificial (Buick et. al, 2004). By studying these phenomena, the numerical ability of the LBM to model the SWRC at the meso-scale and micro-scale can be determined. The single-phase LBM wave propagation investigation occurs at the meso-scale, while the multi-phase LBM density distribution study occurs at the micro-scale. The simulation methods used in this study afford the opportunity to better understand basic mechanisms of drainage and imbibition cycle because the details that can be extracted from simulations remain unavailable from physical tests and from the limited capabilities of LBM-only representation. Furthermore, the static particle configurations in this study is used to

study capillary behavior, and provide a foundation for future research in deformation effects on the SWRC.

## 1.3 Scope and Contributions

Following the introductory Chapter 1, this thesis will continue with Chapter 2, which provides a brief overview of unsaturated soil mechanics, particularly as pertinent to the SWRC. This chapter will also detail the recent literature that discusses the micromechanical modeling of the SWRC.

Following Chapter 2, a detailed description of the DEM-LBM formulation used in this study is provided in Chapter 3. Chapter 4 presents and discusses the results of the simulations conducted in this work. Chapter 5 includes conclusions and recommendation for future research drawn based upon the current study.

The main contributions of this research include providing further insight into the effect of wave propagation in the LBM that has been questioned in the literature, as well as developing a multi-phase LBM model that can not only model the SWRC, but can also show the effects of changes in fluid density distribution. This study also presents a benchmark reference for modeling the SWRC that can be extended in future works to simulations with varying moving particle configurations. Such moving particle simulations could be used to study the effect of deformation on the SWRC, specifically the capillary regime.

# CHAPTER II

# BACKGROUND

## 2.1 Introduction

The purpose of this chapter is to provide a setting in which the need for the research conducted in this work can be clearly seen. The following sections will provide introductory information about unsaturated soil mechanics and its progression in general, the SWRC, and numerical modeling of the SWRC itself.

## 2.2 Unsaturated soil mechanics

Most man-made earth structures involve the use of compacted soils. The compaction process produces a soil with a degree of saturation usually in the range of 75 -90%. Earthen dams, embankments, and highways are typical examples of earth structures made of compacted, unsaturated soils. The omnipresence of unsaturated soils in geotechnical practice underlines the importance of quantifying the soil behavior using state variables and laboratory tests.

Experimental studies in the 1950s, such as Bishop et al. (1960), illustrated the possibility of independent measurement of the pore-water and pore-air pressures by high air entry ceramic disks. Subsequently, over the next decade, further studies concluded that the behavior of saturated and unsaturated soils was fundamentally different. However, these same studies also revealed several problems with laboratory testing of unsaturated soils. Testing was time consuming and demanded precision in the execution

of testing techniques. The difficulty in testing led to a search for a single-valued effective stress equation for unsaturated soils (Fredlund and Delwyn, 2006). However, by the late 1960's Fredlund and his contemporaries became aware that the use of two independent stress state variables would be more consistent with continuum mechanics. For the next decade, an extension of classical soil mechanics concepts, such as the Mohr-Coulomb failure envelope, was developed for unsaturated soils. An example of this envelope is shown in Figure 2.1. The extensions of these models were introduced to include the gaseous phase, and to model soil as a ternary system.

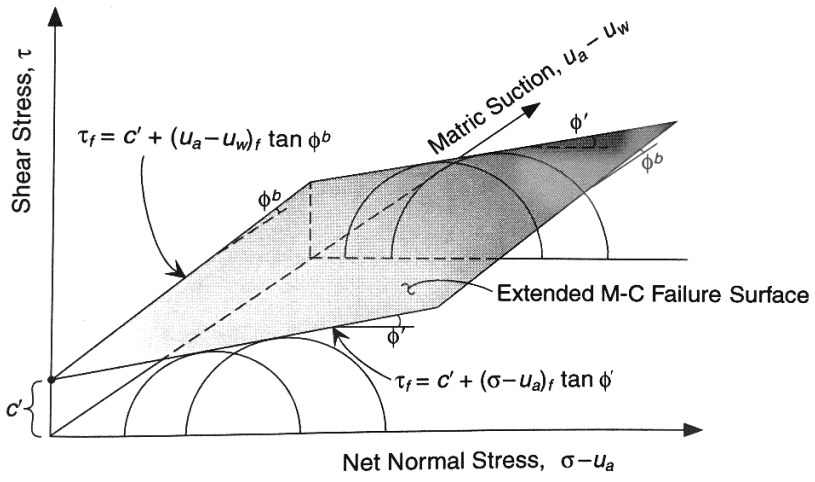


Figure 2.1 Sample planar failure envelope showing the extended Mohr-Coulomb criterion for unsaturated soil (Lu and Likos 2004)

After the constitutive relations stemming from classical soil mechanics were studied in the 1970's, boundary-value problems were solved in the 1980's using numerical, finite element, and finite difference models. The main concern during this time was the saturated-unsaturated seepage model, presenting the first unsaturated soils

problem to come into prominence in the realm of common engineering practice (Fredlund and Delwyn, 2006).

Since the 1990's, unsaturated soil mechanics and its applications to common geotechnical engineering problems has come to the forefront of the research community. A common benchmark topic that is used when proposing new methods for understanding the general behavior of an unsaturated soil is the study of the Soil Water Retention Curve.

## 2.3 Soil Water Retention Curve

The soil water retention curve (SWRC) is a key constitutive relationship to describe the behavior of unsaturated soils. The SWRC provides a relationship between the volumetric water content in the soil specimen and matric suction, the difference between the pore air pressure and pore water pressure. The SWRC can be directly measured in the laboratory or field in a variety of ways. Further, there are several parameterized models in the literature to represent SWRC (e.g., Brooks and Corey 1964; van Genuchten 1980; Fredlund and Xing 1994).

These models establish the relationship between water content and suction using a functional form including several fitting parameters. The level of complexity and the number of fitting parameters differ among these models. The van Genuchten equation can be written as

$$\frac{\theta - \theta_r}{\theta_s - \theta_r} = \left[1 + \left(\frac{h}{h_{vG}}\right)^n\right]^{-m} \tag{2.1}$$

where $\theta$ is the volumetric water content, $\theta_s$ and $\theta_r$, are the saturated water content and residual water content respectively, $h$ is the pressure head with a scaling

parameter $h_{vG}$, and $m$ and $n$ are shape parameters relating the air-entry value and porosity of the soil to the SWRC model. It is possible to reproduce the SWRC with several methods.

One can employ a model to either produce discrete points fit with a modeling equation such as Equation 2.1 or a continuous curve generated from an exact solution. Many experiments have utilized the former, one example being Haverkamp, Randel, et al. (2005). However, both the former and the latter can be done using scaled models of soil skeletons under varying fluid conditions. These models are known as micromechanical models due to the scale that characterizes the design and the governing equations that are deployed in the numerical experiments. It should be noted that only a few select variables can be measured with limited resolution in a physical test and, importantly, it is nearly impossible to measure conjugate variable pairs (e.g. water content and pressure) at the same point. However, these physical tests can be supplemented by micromechanical models.

## 2.4 Micromechanical modeling of the SWRC

The LBM is growing in popularity for multi-phase flow simulations and is particularly attractive when coupled with the DEM, which adds the ability to quantify interparticle stress. One of the main advantages of using this method is the ease at which one can generate models representing processes and effects at the molecular scale such as those producing phase separation and immiscibility.

These physical processes are then incorporated into the macroscopic models of choice through upscaling, as is outlined in Chen and Doolen (1998). The LBM models proposed by Shan and Chen (1993,1994) (S-C), Galindo-Torres et al. (2013), and Martys

and Chen (1996) are of particular interest. These numerical representations are useful for modeling the SWRC because they represent the liquid-vapor phase interface based on repulsive interactions between the fluid molecules themselves, independent of solid contacts and fluid-particle interaction. Coupling the LBM model with the DEM model allows local determination of the interparticle and fluid-particle interactions, thus creating a trajectory to a micromechanical model of unsaturated soil.

Successful examples of such a coupled DEM-LBM model have been presented recently in the geomechanical literature (e.g., Lomine et al., 2013; Sun et al., 2013; Han and Cundall, 2013). However, it has been noted in the literature that wave propagation in the LBM is unavoidable. Be the waves a numerical artifact or physical waves, it is important to examine the effect that these waves have on fluid-solid interactions.

Galindo-Torres et al. (2016) performed a study exploring the LBM's behavior by numerically simulating the SWRC in a small volume as proposed by Schaap et al. (2007). They suggested that the numerical representation of the SWRC with the S-C model is highly sensitive to initial fluid distribution. The present work investigates characteristic factors of the LBM to illustrate in-depth the effects of various numerical parameters on the production of the SWRC. By first quantifying the effect of wave propagation on solid obstacles in the LBM, variables in the study of initial fluid distribution can possibly be eliminated.

As discussed in Fili et al. (2017), it can be shown that in the capillary regime of the SWRC the shape of the wetting front permeating the soil skeleton produces a significant effect on the suction values and shapes of the SWRC. The initialization of the density distribution of both the wetting and non-wetting fluids in the LBM simulation can

be adjusted to model a unified and non-unified wetting front. Furthermore, when the density distributions reach a steady state, the immiscibility of the fluids affords the opportunity to study the effects of changing the aforementioned distribution parameters on the capillary pressure of the enclosed volumes of fluid (Galindo-Torres et al., 2016).

CHAPTER III

FORMULATIONS OF DEM-LBM

## 3.1 Introduction

The following chapter will provide the theoretical background and methodology used to create both the single-phase coupled DEM-LBM method and the multi-phase LBM that was used to conduct the research presented in later chapters.

## 3.2 The lattice Boltzmann method

### 3.2.1 Density distribution functions and time evolution

The lattice Boltzmann method (LBM, Wolf-Gladrow, 2000; Succi, 2001; Rothman and Zaleski, 2004; Sukop and Thorne, 2006) is a simulation technique for solving fluid flow and transport equations. LBM characterizes the fluid at points located on a regular d-dimensional lattice. For a lattice representation DdQz, each point in the D-dimensional lattice links to neighboring points with z links that correspond to velocity directions. For example, the D3Q15 lattice in three dimensions uses fifteen velocity vectors $e_0$ to $e_{14}$, as shown in Fig. 3.1.

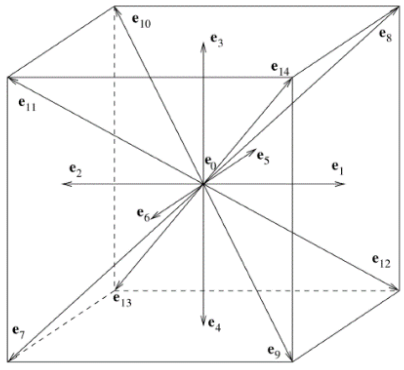


Figure 3.1 D3Q15 lattice velocities

Primary variables of LBM are density distribution functions, $f_i$. Density distribution functions $f_0$ to $f_{14}$, corresponding to velocity vectors $e_0$ to $e_{14}$, represent portions of a local mass density moving into neighboring cells in the directions of discrete velocities. The macroscopic fluid density ρ at each lattice point is a sum of the distribution functions at that lattice point:

$$\rho = \sum_{i=0}^{14} f_i \tag{3.1}$$

Fluid velocity at the lattice point is a weighted sum of lattice velocities, with distribution functions being the weight coefficients:

$$\boldsymbol{u} = \frac{\sum_{i=0}^{14} f_i \boldsymbol{e_i}}{\sum_{i=0}^{14} f_i} = \frac{\sum_{i=0}^{14} f_i \boldsymbol{e_i}}{\rho} \tag{3.2}$$

where $f_i/\rho$ ratio can be interpreted as a probability of finding a particle at a given spatial location with a discrete velocity $\boldsymbol{e_i}$.

Using the collision model of Bhatnagar-Gross-Krook (BGK, Bhatnagar et al., 1954) with a single relaxation time, the time evolution of the distribution functions is given by

$$f_i(r + e_i \Delta t, t + \Delta t) = f_i(r, t) + \frac{1}{\tau_u}\left(f_i^{eq}(r, t) - f_i(r, t)\right), i = 0 \dots 14 \tag{3.3}$$

where $\boldsymbol{r}$ and $t$ are the space and time position of a lattice site, $\Delta t$ is the time step, and $\tau_u$ is the relaxation parameter for the fluid flow. The relaxation parameter $\tau_u$ specifies how fast each density distribution function $f_i$ approaches its equilibrium $f_i^{eq}$. Kinematic viscosity ν is related to the relaxation parameter $\tau_u$, the lattice spacing $\Delta x$, and the simulation time step $\Delta t$ by

$$\nu = \frac{\tau_u - 0.5}{3}\frac{\Delta x^2}{\Delta t} \tag{3.4}$$

Depending on the dimensionality *d* of the modeling space and a chosen set of the discrete velocities $e_i$, the corresponding equilibrium density distribution function can be found (Qian et al.,1992). For the D3Q15 lattice, the equilibrium distribution functions $f_i^{eq}$ are

$$f_i^{eq}(r) = \omega_i \rho(r) \left( 1 + 3\frac{e_i \cdot u(r)}{c^2} + \frac{\frac{9}{2}\left(e_i \cdot u(r)\right)^2}{c^4} - \frac{\frac{3}{2}u(r) \cdot u(r)}{c^2} \right) \tag{3.5}$$

with the lattice velocity $c = \Delta x/\Delta t$ and the weights

$$\omega_i = \begin{cases} \frac{2}{9} & i = 0 \\ \frac{1}{9} & i = 1 \dots 6 \\ \frac{1}{72} & i = 7 \dots 14 \end{cases} \tag{3.6}$$

Using the Chapman-Enskog expansion (Chapman and Cowling, 1970), it can be shown that LBM Eqs. 3.3 to 3.6 provide an approximation of the incompressible Navier-Stokes Eqs. 3.7 to 3.8 without external forces:

$$\rho \left[ \frac{\partial u}{\partial t} + u \cdot \nabla u \right] = \nabla \cdot (\mu \nabla u) \tag{3.7}$$

$$\nabla \cdot u = 0 \tag{3.8}$$

where the $\mu = \nu\rho$ is the dynamic viscosity of fluid. This approximation is valid in the limit of low Mach number $M = |\boldsymbol{u}|/c$, with a compressibility error on the order of $\sim M^2$ (Succi, 2001).

## 3.3 Multi-phase extension of LBM

Because unsaturated soil is a ternary system, it is necessary to extend the above model into a multi-phase DEM-LBM model. A multi-phase extension of lattice-Boltzmann method (LBM) provides a valuable numerical model for soil specimens subjected to external forcing conditions (Schaap et al., 2007; Galindo-Torres et al., 2016). In this work, a single-component, multi-phase LBM system was developed using an in-house code to simulate transient flow processes including pore water in partially saturated soils.

#### 3.3.1.1 Fluid interaction

LBM models fluid cohesion in multi-phase flows by introducing interaction forces between the particles of fluid. Using the method outlined in Shan, Chen (2013), the governing force on the fluid particles in absence of solid boundaries or obstacles is comprised solely of attractive (cohesive) forces between the fluid particles presented in Equation (3.9). The attractive force is based on an "interaction potential", ψ which is proportional to the density of fluid in a fluid cell under examination, as given by Equation (3.10).

$$F_a = -G_a\psi(x)\sum_{i=1}^{15}\omega_i\psi(x+\Delta t e_i)e_i \tag{3.9}$$

$$\psi = \psi_0 exp\left(\frac{-\rho_0}{\rho}\right) \tag{3.10}$$

The sum is performed over all neighboring cells, where $G_a$ is a parameter representing strength of cohesive interaction and $\omega_i$ are weight coefficients (Equation 3.6), while $\psi_0$ and $\rho_0$ are interaction potential parameters.

In the presence of a solid boundary or particulate obstacle, the attractive (adhesive) force between the fluid and solid particles is given by

$$F_s = -G_s\psi(x)\sum_{i=1}^{15}\omega_i s(x + \Delta t e_i)e_i \tag{3.11}$$

An external force is incorporated as:

$$F_g = \rho g \tag{3.12}$$

where g is a body force that is equivalent to the gravitational acceleration for a system in the gravitational field.

#### 3.3.1.2 Immiscibility and mixing of fluids

A multi-phase fluid in the lattice-Boltzmann model is represented by introducing additional density distribution for each additional fluid component. In case of a two-component fluid, the densities of individual components are marked $\rho_1$ and $\rho_2$. Each fluid component has its own $G_a$and $G_s$ coefficients as described earlier by Equations (3.9) and (3.11). Furthermore, the two fluid components are also under the influence of a repulsive force:

$$F_r = -G_r\rho_1(x)\sum_{i=1}^{15}\omega_i\rho_2(x + \Delta t e_i)e_i \tag{3.13}$$

where strength of the repulsive interaction is characterized by a coefficient $G_r$. The values of these coefficients can be determined based on the fluid densities desired for the simulation design. Once the initial densities are chosen, the miscibility of the fluid

components depends on the product $\rho_t G_r$, where $\rho_t$ is the sum of the individual fluid densities:

$$\rho_t = \rho_1 + \rho_2 \tag{3.14}$$

Two fluid components will separate if

$$\rho_t G_r \leq \rho_t G_r^{critical} \tag{3.15}$$

or will mix otherwise (Schaap et al., 2007). Individual fluid densities are initialized to 0 and 1, respectively. A critical range for $\rho_t G_r$ between 0.8 and 1.1 (lattice distance) x (mass units) was found, enabling determination of the other force coefficients listed above to prevent thin films from forming.

Total effective velocity of a mixture is calculated as a weighted sum of individual fluid velocities

$$u = \frac{\sum_\sigma \frac{1}{\tau_\sigma} \sum_{i=1}^{15} f_i^\sigma e_i}{\sum_\sigma \frac{\rho_\sigma}{\tau_\sigma}} \tag{3.16}$$

where the index $\sigma$ enumerates fluid components. After all contributing forces are added to the total force on a fluid particle, the velocity of the fluid particle is updated as follows:

$$u' = u + \frac{\Delta t F}{\rho} \tag{3.17}$$

#### 3.3.1.3 Fluid phase pressure

To find the total fluid pressure, $P(\vec{x})$ at any point in an LBM cell sharing two fluids, the following is used:

$$P(\vec{x}) = \frac{\rho_1 + \rho_2 + G_r \rho_1 \rho_2}{3} \tag{3.18}$$

Then, as in Galindo-Torres (2015), the pressure of each phase is found by calculating the average pressure of the cells enclosed by each fluid volume. The difference of Equation 3.18 and this pressure will give the capillary pressure of the phase in question.

### 3.3.2 Immersed moving boundary

The immersed moving boundary (IMB) technique (Noble and Torczynski, 1998; Strack and Cook, 2007; Owen et al., 2011) allows solid boundaries to move through the computational grid. The IMB method introduces a subgrid resolution at the solid-liquid boundaries, resulting in smoothly changing forces and torques exerted by the fluid on moving particles. The IMB introduces an additional collision operator $\Omega_i^S$ expressing collisions of solid particles with fluid as

$$\Omega_i^S = f_{-i}(r,t) - f_i(r,t) + f_i^{eq}(\rho, U_S) - f_{-i}^{eq}(\rho, u) \tag{3.19}$$

The time evolution of the density distribution functions in IMB includes $\Omega_i^S$

$$f_i = f_i(r,t) + [1-\beta(\epsilon,\tau)]\frac{1}{\tau}\left(f_i^{eq}(r,t) - f_i(r,t)\right) + \beta(\epsilon,\tau)\Omega_i^S \qquad \mathrm{i} = 0{:}\,14 \tag{3.20}$$

where the weighting factor $\beta(\varepsilon,\tau)$ depends on solid coverage $\varepsilon$ and relaxation parameter $\tau$

$$\beta(\epsilon,\tau) = \frac{\epsilon}{1 + \frac{1-\epsilon}{\tau - 0.5}} \tag{3.21}$$

### 3.3.3 Fluid force on particles

The total hydrodynamic force exerted by the fluid on a particle is calculated by summing the momentum change at every lattice cell due to the new collision operator:

$$F_F = \frac{\Delta x^3}{\Delta t} \sum_n \left( \beta_n \sum_{i=0}^{14} \Omega_i^S e_i \right) \tag{3.22}$$

### 3.3.4 Boundary conditions

At the fluid-solid interface, the "no-slip" boundary condition is imposed, which is a prevalent choice with IMB technique (Cook et al., 2004; Feng and Michaelides, 2004; Strack and Cook, 2007; Owen et al., 2011).

At the outer boundaries of the simulation domain, the boundary condition for fluid can be periodic or non-periodic. Non-periodic boundary conditions can impose a constant velocity, simple wall (bounce-back), partially covered wall (immersed boundary), or moving wall (immersed moving boundary). Moving walls can be

• velocity driven - moving with a prescribed velocity,

• force driven - driven by a sum of fluid force, particle forces, and an external constraining force.

Constant velocity boundary condition (BC), following the work of Zou and He (1997), can be applied at the inlet/outlet boundary. An alternative is to apply body force, what is equivalent to applying an external pressure gradient.

## 3.4 The discrete element method

The DEM is a robust numerical method that was originally developed by Cundall and Strack (1979) to simulate dry granular materials. Since then, the method and its subsequent developments have been extensively used for simulating various problems in geomechanics. The DEM treats particles as distinct interacting bodies that are governed

locally by contact laws that control particle interpenetration and dissipate energy. Examples of contact interactions behavior are given by Cole and Peters (2008). An example of a contact law is the power law model that is evaluated for contact overlap (Owen 2011) and is written as:

$$F_N = \alpha K_N \delta_n^m \tag{3.23}$$

where α and m are power law parameter with α=m=1 for the linear contact law, $K_N$ is the normal stiffness, and δ is the penetration distance. In this study, simple linear contact laws are used, but with differing moduli used for loading and unloading to represent energy dissipation.

After determining the contact forces on each particle, the particle velocity and angular rotation are determined by integrating Newton's equations of motion. The equations of motion are expressed as:

$$m\frac{\partial v_i}{\partial t} = mgn_i^g + \sum_{c=1}^{N_c} f_i^c \tag{3.24}$$

and

$$I_m\rho\ \frac{\partial \omega_i}{\partial t} = \sum_{c=1}^{N_c} e_{ijk} f_i^c r_j^c + \sum_{c=1}^{N_c} M_i^c \tag{3.25}$$

where $m$ and $I_m$ are the particle mass and moment of inertia respectively, $gn_i^g$ is the acceleration of gravity, $f_i^c$ is the force term for the particle, $M_i^c$ is the moment term for the particle, and $N_c$ is the number of contacts.

## 3.5 Coupled DEM-LBM

The discrete element method (DEM) subsystem of the DEM+LBM coupled system is described in Peters et al. (2010). The DEM subsystem accounts for the effects of fluid by simply adding forces and torques exerted on particles by fluid to the total DEM contact forces. The LBM subsystem of the coupled system resolves the motion of fluid between particles and evaluates forces and torques exerted by fluid on particles. The forces and torques exerted by fluid on particles are then passed to the DEM subsystem, which performs integration of equations of motion for particles by applying total (DEM+LBM) forces and torques.

### 3.5.1 The DEM-LBM coupling cycle

The DEM+LBM coupling is performed in a cycle as follows:

1.) DEM calculates contact forces and torques between particles/objects.

2.) LBM receives locations and velocities of particles/objects from DEM.

3.) LBM utilizes

3.1) state of the fluid flow from the previous step,

3.2) new locations and velocities of the particles/objects from DEM,

3.3) boundary conditions to calculate fluid velocities on a cubic grid.

4.) LBM calculates forces and torques exerted by fluid on particles/objects.

5.) LBM adds fluid forces and torques to DEM's contact forces and torques.

6.) DEM integrates equations of motion and updates locations and velocities of particles/objects.

### 3.5.2 Multi-stepping

The LBM time step $\Delta t$ is determined from the kinematic viscosity of fluid $v$, required grid resolution $\Delta x$, and constraints on the relaxation parameter ($\tau$ >0.5) according to Eq. 3.4. The relaxation parameter must be chosen low enough to achieve a sufficient time resolution. An upper limit on the relaxation parameter is given by the low Mach number constraint. For DEM, the largest acceptable time step value is determined from the smallest particle mass $m_i$ and the stiffest spring $k_i$ in the system, given the frequency of fastest oscillations

$$\omega_{max} = \sqrt{\frac{MAX(k_i)}{MIN(m_i)}} \tag{3.26}$$

and their time period

$$T_{min} = \frac{2\pi}{\omega_{max}} \tag{3.27}$$

In this work, the LBM time step is constrained to be greater than or equal to the DEM time step. Accordingly, the LBM time step is determined first, and then the DEM time step is adjusted to perform an integer number of DEM substeps before performing the LBM calculation.

To couple the two methods, the DEM first calculates contact forces and torques between the particles. The LBM then receives the locations and velocities of the particles and solves the fluid equations. The LBM calculates the fluid forces and torques on the particles at the current positions and adds those forces and torques to the DEM's contact forces and torques. Finally, the DEM integrates the equations of motion and updates the locations and velocities of the particles. It should be noted that during the DEM

subcycling, the fluid forces and torques remain constant, and the fluid-solid boundary does not move. Therefore, care must be taken when deciding the number of DEM subcycles (Owen *et al.,* 2011).

# CHAPTER IV

# RESULTS AND DISCUSSION

## 4.1 Introduction

Using the coupled DEM-LBM and multiphase LBM outlined in the previous chapter, the numerical experiments detailed in this chapter were used to examine the performance of each method. Furthermore, key parameters were studied to determine the extent of their influence on the simulation of SWRC's. This chapter will first discuss the DEM-LBM and its use in the wave propagation experiments. Then, the multi-phase LBM validation and density distribution experiments will be discussed.

## 4.2 DEM-LBM and wave propagation

To quantify the effect of wave propagation and to establish whether the observed waves stemming from initialization have a physical meaning in the DEM-LBM method, a single particle simulation was designed. Snapshots of this simulation are shown in Fig. 4.1.

### 4.2.1 Model setup

Table 4.1 Input parameters used in the DEM-LBM settling particle simulation

| Property | Units | Value |
|---|---|---|
| Particle Radius | mm | 1.0 |
| Fluid Viscosity | Pa-s | $1.0\ E^{-6}$ |
| Fluid Density | kg/m$^3$ | 1000 |
| Grid Distance | m | $9.9\ E^{-5}$ |
| Domain Dimensions | mm | 20 x 80 x 1 |

The particle was placed under in the influence of gravity and with an initial zero velocity in all directions. The parameters used in this study, which can be found in Table 4.1, were chosen based on the significant role that Equation 3.4 plays in the DEM-LBM

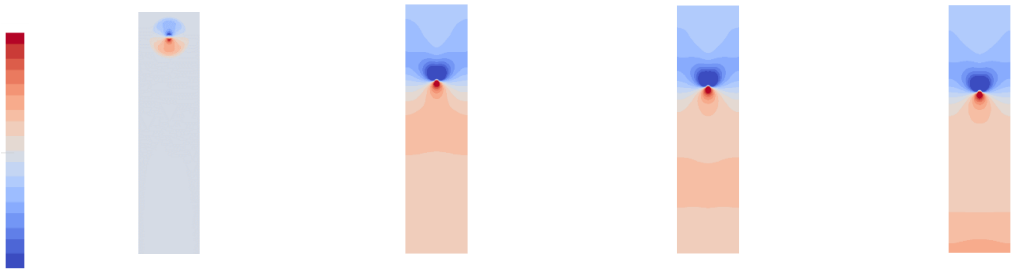

Figure 4.1 An example of the gravity-capillary wave propagating through the domain as a single particle falls in a fluid-filled shaft.

formulation. These parameters also were chosen to reflect the analytical solution of a settling particle in water as closely as possible. The x, y, z-dimensions of the domain are 20mm x 80 mm x 1 mm, with a periodic boundary condition in the z direction. The ratio of grid distance to time step, $\frac{\Delta x}{\Delta t}$, or LBM lattice speed, for this study was set initially as in Fili et al. (2017), with a grid distance of 9.90E-05 m, and then increased by 1.25x, 1.5x, and 2.0x. By varying the grid distance in the simulation, the rate at which each fluid density distribution function $f_i$ approaches its equilibrium $f_i^{eq}$ will be changed (Equation 3.3-3.6). By keeping the physical parameters constant, but changing the above, the waves in the LBM will be represented on different scales proportional to the grid distance. Thusly, a trend between the grid distance and effect of wave propagation can be observed.

### 4.2.2 Results and discussion

As the grid distance of the settling particle was varied, a study of particle velocity and force on the particle was conducted. All settling particle simulations approach the analytical solution for terminal velocity for a falling particle in a fluid using the Immersed Moving Boundary LBM method, similarly to a classing drafting-kissing tumbling (DKT) case. More information about DKT and the solutions can be found in Feng and Michaelides (2004). Figure 4.1 shows a plot of the particle velocity in the y-direction, the direction of motion in the settling particle simulation. The grid distance was varied as mentioned above and plotted with a convention relative to the particle diameter, with $\frac{d}{\Delta x}$ values of 20.1, 16.2, 13.4, and 10.1, where d is the particle diameter and $\Delta$x is the LBM grid distance. For convenience, these values are rounded in Figure 4.1 and the remainder of this chapter. As evidenced by the plot, varying grid distance has minute effect on the velocity of the particle.

In a similar plot of the fluid force on the particle, Figure 4.2, it is immediately apparent that grid distance influences the noise present in the force solution. At the initialization, there are sharp changes in force that attenuate quickly as the fluid motion reaches equilibrium with particle velocity. At the initialization of many LBM simulations, as discussed in Buick et al. (2004), the fluid will exhibit behavior that can be attributed to wave propagation through the domain. Upon detailed examination, force evidence of the effect of wave propagation from the particle as a source can be seen in this simulation. Figure 4.3 contains a subsection of the forces on the particle plotted in Figure 4.2.

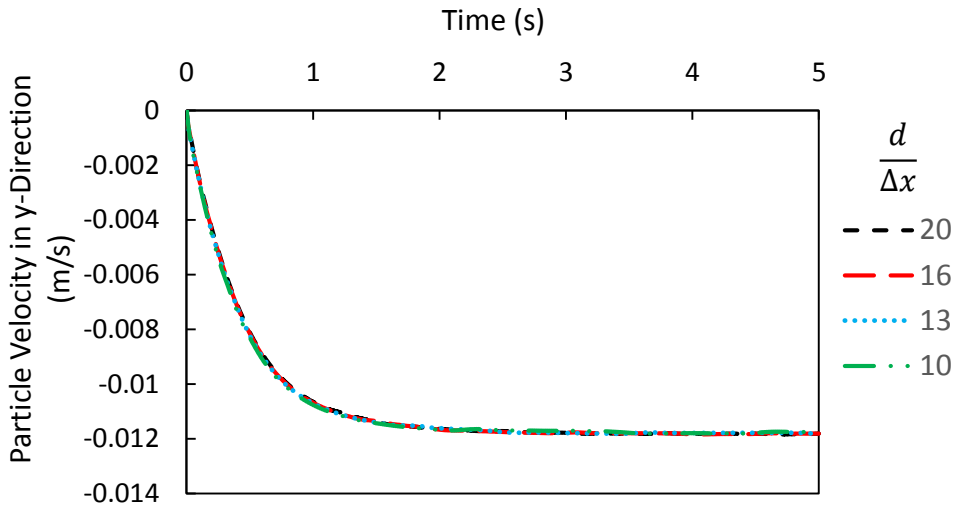


Figure 4.2 Velocities of particles in settling-particle simulations versus time

After the particle begins to move through the fluid domain, there are clear increases in force towards the bottom of the simulation domain. The coarseness of the grid affects these localized minima. As the grid becomes coarser, i.e. the grid distance of the LBM is increased, the time at which the minima occur happens later in the simulation. This is due to the change in lattice speed that arises from changing the grid distance, which in-turn will affect the relaxation time of the simulation (Equation 3.4). The grid distance affects the placement and amplitude of the local minima in the fluid force on the particle, meriting the analysis of their correlation.

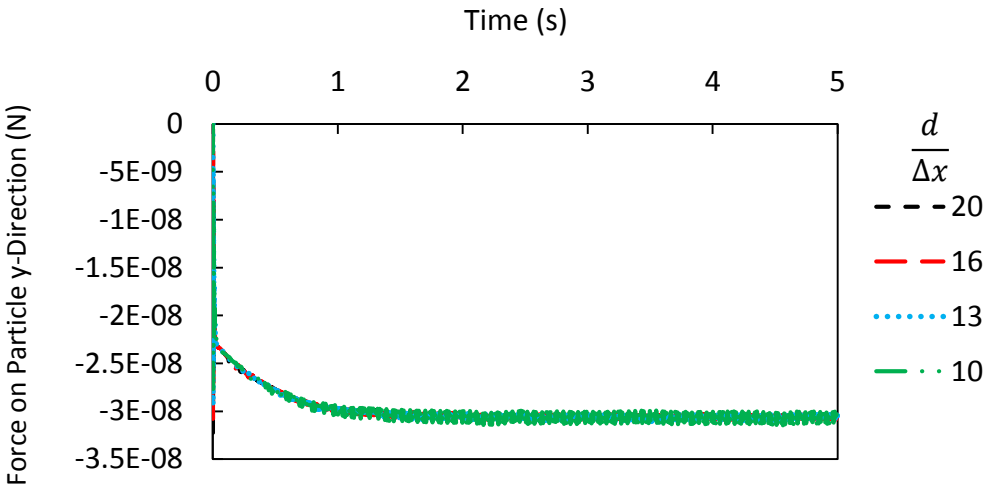


Figure 4.3 The fluid forces on each settling particle, y-component.

The wave propagation in this work could be attributed to two types of waves: artificial and capillary. Artificial waves arise from the LBM method, as discussed in Buick et al. (2004). Capillary waves are caused by surface tension forces and rapid changes in fluid density across the LBM grid. Solid particle movement in the DEM-LBM across the fluid grid causes such a rapid change in density. To confirm the changes in force on the particle resulted from the propagation of a density wave from the particle, a density distribution study was conducted. Density profiles were generated by sampling the densities across in the x-center of the domain and plotting them versus the y-, as shown in Figure 4.4.

Because the single-particle simulation employs the IMB method, the fluid within the particle is under the influence of gravitational force, but remains confined by the particle itself. The IMB method introduces a subgrid resolution at the solid-liquid boundaries, resulting in smoothly changing forces and torques exerted by the fluid on moving particles. As such, the density profiles for different $\frac{d}{\Delta x}$ ratios shown in Figure 4.4

yield a smooth density transition after an initial sharp increase. The sharp increase denotes the bottom edge of the particle, with a linear decrease trough the diameter of the particle, until the density returns to its equilibrium value outside of the particle. The distinct shape of these density profiles affords the opportunity to clearly observe the propagation of any capillary waves. The fluctuation in density outside of the particle is evidence of such a propagation. The small increases in density to the left of each peak in Figure 4.4 illustrate this phenomenon. Furthermore, the profiles generated in Figure 4.4 correspond to the same time at which the minima occur in Figure 4.3.

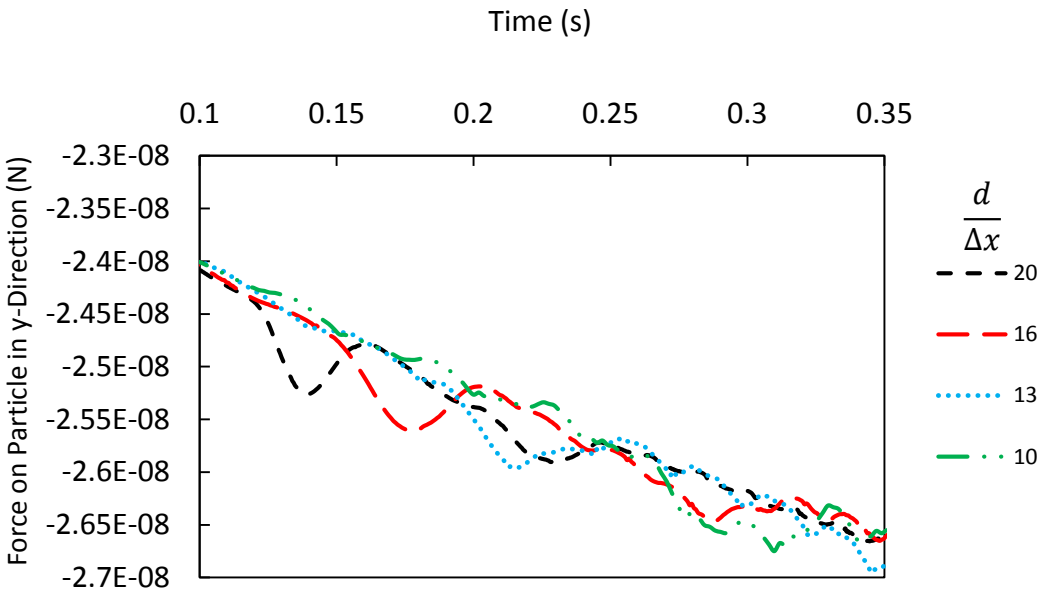


Figure 4.4 Enlarged section of Figure 4.6, from t = 0.1-0.35 s.

Further substantiation of the presence of physical wave propagation can be obtained by isolating a single simulation and refining the time scale. This is shown in Figure 4.5. At t = 0.01s, the density profile consists only of the change in density across the diameter of the solid particle.

However, at t = 0.05s, a perturbation can be seen around both y = 0.0675m and y = 0.0775 m. This shows a wave propagating outwardly from the particle center in the direction of the top and bottom of the simulation domain. One would expect to see, at this smaller scale, such a wave reflecting from the solid "ceiling" boundary of the LBM domain as time progresses, as observed at t = 0.11 s at y = 0.075 m. In addition, the wave that originated

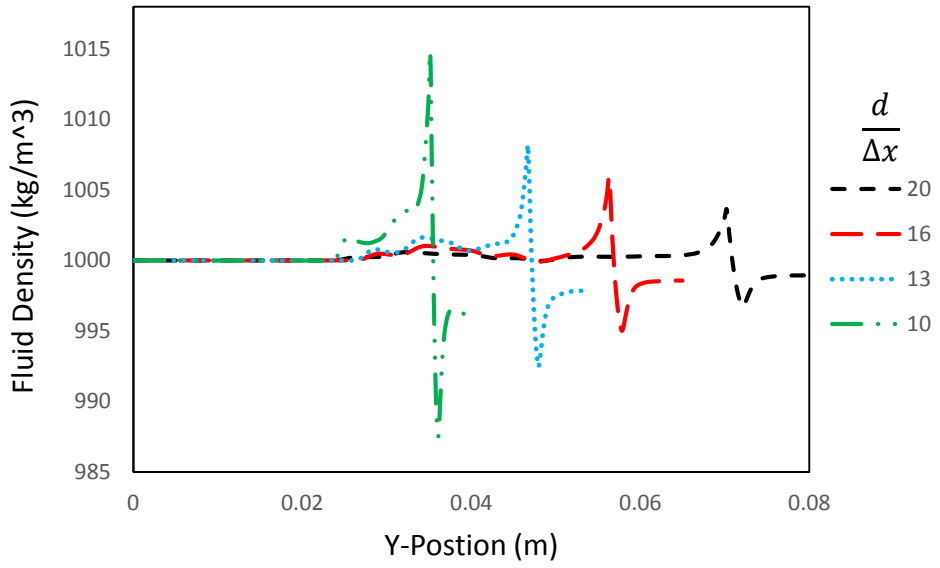


Figure 4.5 Average fluid density versus y-position of particle in the domain.

from the bottom of the particle can also be seen at t = 0.11 s at y = 0.06 m. By examining the density profile at the corresponding time of the local fluid force minima in the beginning of the simulations, it is clear that wave propagation influences the force and, consequently, on the fluid pressure that acts on the particle, though small in value. It is also clear that to minimize the effect of this wave propagation, a finer grid that closely

matches analytical solution must be chosen. But, most importantly, the results show that though the waves propagating in the fluid are indeed caused by the initialization process and the LBM itself, they do hold a physical significance.

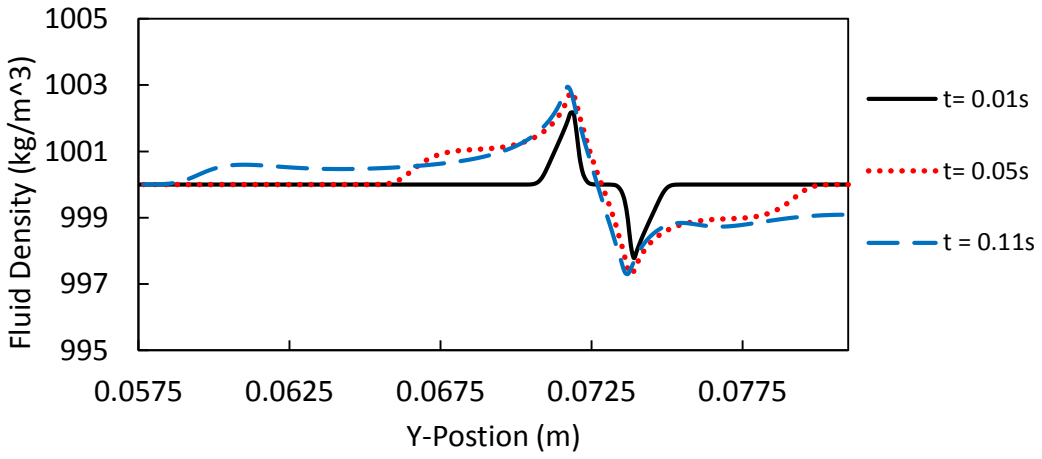


Figure 4.6 Average fluid density versus y-position of particle in domain. Time progression.

## 4.3 Multiphase LBM validation

In this work it is important to validate the LBM model, particularly with respect to the governing forces controlling the movement of the gaseous and liquid phases of the fluid. More details about the S-C model and the attractive, repulsive, and adhesive forces can be found in Galindo-Torres et al. (2016). To test the implementation of the above multi-phase LBM extension, several simulations were executed.

### 4.3.1 Model setup

#### 4.3.1.1 Fluid interaction

First, a cubic domain was generated in the LBM with dimensions of 50x50x50 mm. The single-phase fluid was initialized with a random distribution over the entirety of

the domain. This can be seen in the top left portion of Figure 4.6. At time t > 0, the forces, including gravity and cohesion force were introduced to the fluid allowing the fluid to coalesce into large bubbles at equilibrium (Equations 3.9 and 3.10).

The same was then done with a multi-phase fluid with dimensions of 50x50x5 mm with a periodic boundary condition in the z-direction, which is shown in Figure 4.7.

Table 4.2 Input parameters used in the multiphase validation

| Property | Units | Value |
|---|---|---|
| Particle Radius | mm | 10 |
| $G_a$ | ------ | $-200$ |
| $G_s$ | ------ | 200 |
| $G_r$ | ------ | 0.01 |
| Initial Fluid Density | kg/m$^3$ | 500 |
| Grid Distance | m | $9.9\ E^{-5}$ |
| Domain Dimensions | mm | 50 x 50 x 50 |

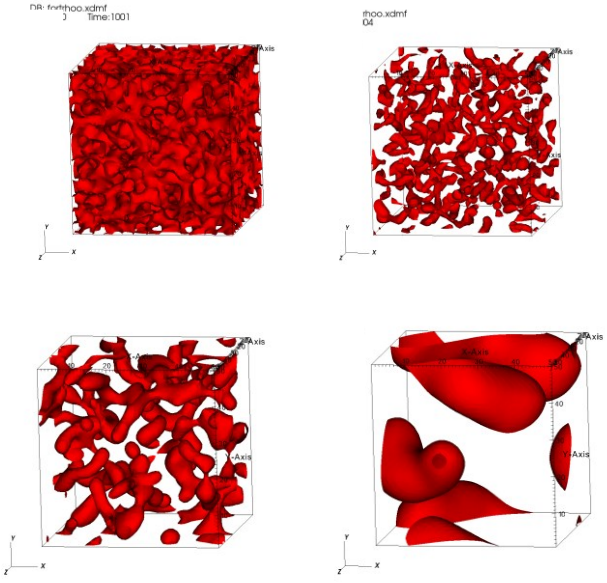

Figure 4.7 Simulation beginning with fluid density distribution randomized at initialization (red). As the simulation progresses, the intermolecular attractions of the fluid cause cohesion as shown.

#### 4.3.1.2 Fluid-solid interaction

In a similar way, at time t > 0, the forces, including gravity, adhesion force, and the cohesion force were introduced to the fluid allowing the fluid to not only to coalesce, but to cover the solid elements of the simulation. This is shown in Figure 4.8. Table 4.2 lists the parameters that were used to design these simulations.

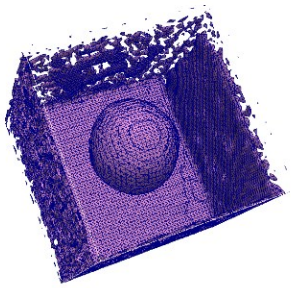

Figure 4.8 3D single particle simulation showing the adhesion behavior of the fluid to the solid particle and to the solid walls of the specimen

### 4.3.2 Results and discussion

As shown by Figure 4.6 and 4.7, the liquid phase of each fluid was able to coalesce successfully into “bubbles” in the simulation domain. These results show that the intermolecular forces between the mesoscale fluid “molecules” are exhibiting attraction independent of each other and acting only between fluid like molecules.

Furthermore, by introducing a solid particle into an LBM simulation, Figure 4.8 shows fluid adhesion to arbitrary solid surfaces, which are present in actual soils, validating the method outlined in Chapter 3 Section 3 of this work.

## 4.4 Static particle array and SWRC generation

### 4.4.1 Model setup

Table 4.3 Input parameters used in the static particle simulations

| Property | Units | Value |
|---|---|---|
| Particle Radius | mm | 4.75 |
| Porosity | ------ | 0.45 |
| Initial Fluid Density | kg/m$^3$ | 500 |
| Grid Distance | m | $9.9\ E^{-5}$ |
| Domain Dimensions | mm | 50 x 100 x 1 |
| $G_a$ | ------ | $-200$ |
| $G_s$ | ------ | 200 |
| $G_r$ | ------ | 0.01 |

After validating the multi-phase LBM model, two types of simulation were performed to quantify the effects of initial density distributions of the wetting fluid on static particles. The simulations used in this work both consist of a rectangular domain populated with an array of cubically packed spherical particles. As with Galindo-Torres et al. (2016) and Fili et al. (2017), a small domain containing five particles in each direction was generated by the DEM and subsequently filled with both phases of the fluid.

The fluids were initialized in the following two ways with respect to the wetting fluid. The first way dispersed the fluid with random density distribution (Figure 4.9), while the second approach introduced the fluid as a droplet confined to a radius of 10 mm (Figure 4.10). Both specimens use boundary conditions that are periodic in the z-direction with flow enabled, and a solid boundary in each x and y-direction. The flow boundary condition is imposed by using a variation of the velocity conditions detailed in Zou and He (1997), in which a zero-velocity profile is initialized, allowing body forces on only

the liquid phase of the fluid to dominate the movement and produce a proper imbibition phase.

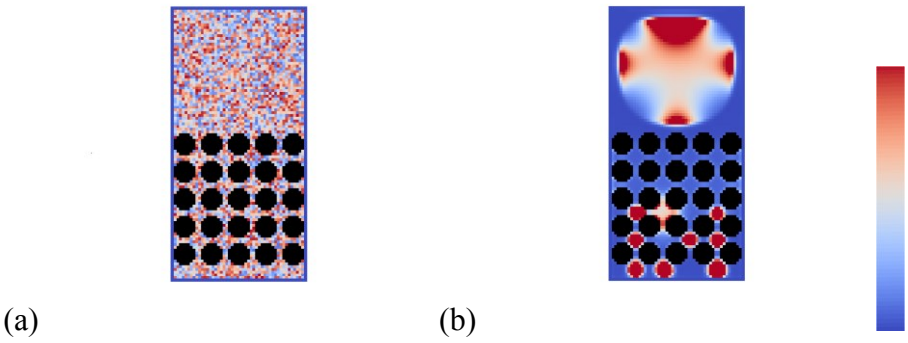

(a) (b)

Figure 4.9 The randomized initial density simulation showing the values of $\rho_1$, the density of the wetting fluid in blue and $\rho_2$, the density of the non-wetting fluid in red. (a) Initial step. (b) Final step.

An external gravitational force was applied in the -y direction. The droplets that formed in both cases percolated between particles in the direction of gravity and spread into the void region of the particle domain.

### 4.4.2 Results and discussion

The LBM grid distance for these simulations was chosen to minimize noise in fluid pressure calculation stemming from wave propagation based on the results in section 4.2.2 and to mirror physical parameters as evaluated by Schaap et al. (2007). The static particle simulations shown Figure 4.9 and Figure 4.10 were then used to generate the SWRC's shown in Figure 4.11. Fluid pressure of each phase was determined using the method outlined in Section 3.1.1.3., and volumetric water content was determined by using a Boolean cell counting scheme in the multi-phase LBM code.

Because the droplet of wetting fluid is confined to an initial radius with given density, the surface tension causes a greater pressure within the bubble than that of the smaller bubbles that eventually coalesce in the randomized initial density simulation. These smaller bubbles are free from a spatial restriction, and as such reach equilibrium both locally and globally more quickly. The results of these physical processes yield a similar trend, but a greater capillary response from the droplet simulation, as shown in Figure 4.11.

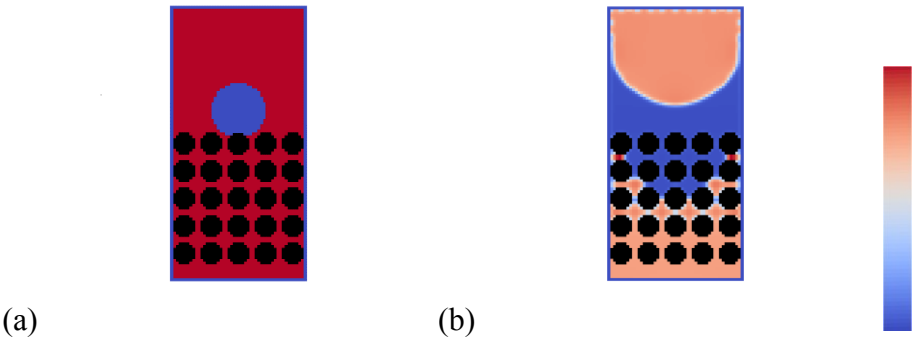

(a) (b)

Figure 4.10 The "droplet" density simulation showing the values of $\rho_1$, the density of the wetting fluid in blue and $\rho_2$, the density of the non-wetting fluid in red. (a) Initial step. (b) Final step.

The volumetric water content of each simulation varies in scale due to the random density initialization in Figure 4.3. The random nature results in a soil skeleton that is partially saturated from $t < 0$, but to a greater degree than the droplet simulation in Figure 4.9 is partially saturated. However, though the range of volumetric water content varies, the peak values for capillary pressure show a pronounced difference in the role that the shape of the wetting front, and in-turn the initial density distribution have on the generation of the SWRC.

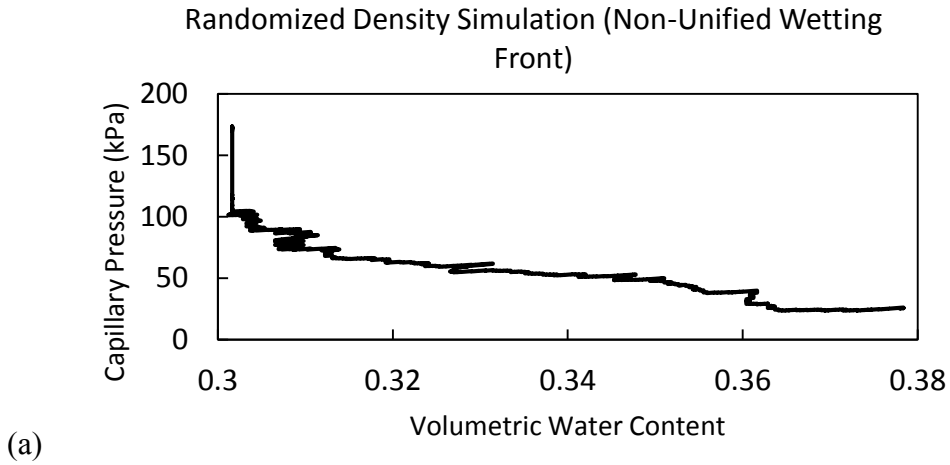


(a)

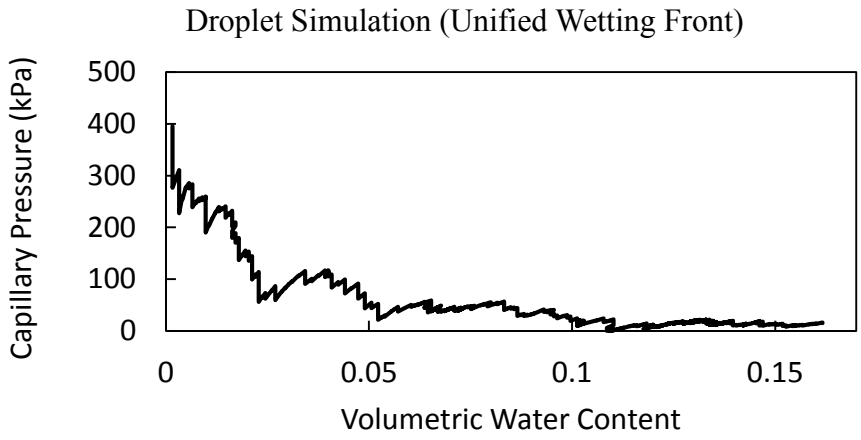


(b)

Figure 4.11 Capillary pressure versus the volumetric water content for the a) droplet simulation and b) randomized density simulation. Porosity of the specimen is n = 0.45

# CHAPTER V

# CONCLUSION

## 5.1 Conclusions

Because wave propagation in the LBM is unavoidable, be the waves a numerical artifact or physical waves, it is important to examine the effect that these waves have on fluid-solid interactions. If waves generated in the presented DEM-LBM method are simply numerical artifacts, it follows logically that the method is unsuitable for the meso- and micro-scale and, by extension, to micromechanical modeling of the SWRC. If said waves are physical, improper scale representation could cause noise in the generation of the SWRC by interfering with the calculation of the fluid pressure in an enclosed volume of fluid phase, which is based on the density of each phase. This study has shown that in the DEM-LBM method, the waves observed in simulations are not an artifact of the method, but physical waves that are dominated by surface tension forces based on density, called capillary waves. It has also shown that by refining the LBM grid, this effect can be minimized by better representing the scale of the physical waves, ensuring the accuracy of SWRC generation.

Furthermore, the effect of density distribution on the generation of the SWRC has been shown to be linked to the shape of the wetting front as it progresses through the soil skeleton. The unified wetting front produces higher peak capillary pressures, but both the unified and non-unified wetting fronts produce a trend in the SWRC that is both easily recognizable and qualitatively expected. This study also presents a benchmark reference in the SWRC that will be extended in future works to simulations with varying moving

particle configurations to study the effect of deformation on the SWRC, specifically the capillary regime.

## 5.2 Recommendations for future research

To provide a more thorough analysis of the effects that the parameters in this study have on the LBM, the development of a non-isothermal, multi-phase DEM-LBM model should be considered. This model would provide a valuable insight into the effect of temperature on the progression of the wetting front through the soil skeleton for varying initial fluid density distributions.

Also, larger particle array simulations that are under load should be considered. This would extend the capability of the present model to represent a multi-phase, unsaturated particle system that can be applied to analyze the effect of deformation of the sample on the SWRC at the microscale.

# REFERENCES


Bhatnagar, P. L. Gross, E. P., and Krook, M., (1954) “A Model for Collision Processes in Gases. I. Small Amplitude Processes in Charged and Neutral One-Component Systems.” *Physical Review*, 94: 511–525.

Bishop, Alan W., et al. (1960) "Factors controlling the strength of partly saturated cohesive soils."

Buick, J. M., Cosgrove, J. A., and Greated. C. A., (2004) "Gravity-capillary internal wave simulation using a binary fluid lattice Boltzmann model." *Applied Mathematical Modelling* 28.2: 183-195.

Chapman, S. and Cowling, T. G., (1970) The *Mathematical Theory of Non-uniform Gases: An Account of the Kinetic Theory of Viscosity, Thermal Conduction and Diffusion in Gases*. Cambridge University Press

Chen, Shiyi, and Gary D. Doolen. (1998) "Lattice Boltzmann method for fluid flows." *Annual review of fluid mechanics* 30.1: 329-364.

Cook, B. K., Noble, D. R. and Williams. J. R., (2004) “A direct simulation method for particle-fluid systems.” *Engineering Computations*, 21 (2/3/4): 151–168.

Cundall, P. A., Strack, O. D. L. (1979). “A discrete numerical model for granular assemblies.” *Géotechnique*, 29(1): 47–65.

Feng, Z.-G. and Michaelides, E. E., (2004) “The immersed boundary-lattice Boltzmann method for solving fluid–particles interaction problems.” *Journal of Computational Physics*, 195 (2): 602–628.

Fili, J. F., Vahedifard, F., Jelinek, B., Peters, J. F. (2017). “Examination of Capillary Regime in the Soil Water Retention Curve using Coupled DEM-LBM Modeling”. *Pan-Am UNSAT 2017, Second Pan-American Conference on Unsaturated Soils: Unsaturated Soil Mechanics for Sustainable Geotechnics*, November 12-15, 2017, Dallas, TX.

Fredlund, D. G. and Rahardjo, H. (1993). Soil Mechanics for Unsaturated Soils, John Wiley & Sons, Inc., New York, 517 pp.

Fredlund, D. G., Sheng, D., and Zhao, J. (2011). “Estimation of soil suction from the soil-water characteristic curve.” Canadian Geotechnical Journal, 48,186-198.

Fredlund, D. G., Xing, A., Fredlund, M. D., & Barbour, S. L. (1996). The relationship of the unsaturated soil shear to the soil-water characteristic curve. Canadian Geotechnical Journal, 33(3), 440-448.

Fredlund, Delwyn G. (2006)"Unsaturated soil mechanics in engineering practice." Journal of geotechnical and geoenvironmental engineering 132.3:286-321.

Galindo-Torres, S. A., et al., (2013) "A Lattice Boltzmann model for studying transient effects during imbibition–drainage cycles in unsaturated soils." *Computer Physics Communications* 184.4: 1086-1093.

Galindo-Torres, S. A., Scheuermann, A., Li, L., (2016) "Boundary effects on the Soil Water Characteristic Curves obtained from lattice Boltzmann simulations." *Computers and Geotechnics*, 71, 136-146.

Han, K., Feng, Y. T., and Owen, D. R. J., (2007) "Coupled lattice Boltzmann and discrete element modelling of fluid-particle interaction problems." *Computers & Structures*, 85 (11–14): 1080–1088

Han, Yanhui, and Peter A. Cundall., (2013) "LBM–DEM modeling of fluid–solid interaction in porous media." International Journal for Numerical and Analytical Methods in Geomechanics 37.10:1391-1407.

Jelinek, B., Eshraghi, M., Felicelli, S., and Peters. J. F., (2014) "Large-scale parallel lattice Boltzmann—cellular automaton model of two-dimensional dendritic growth." *Computer Physics Communications*, 185 (3): 939–947.

Johnson, D. H., Vahedifard, F., Jelinek, B., Peters, J. F. (2017). "Micromechanical Modeling of Discontinuous Shear Thickening in Granular Media-Fluid Suspension". *Journal of Rheology*, 61(2), 265-277.

Johnson, D. H., Vahedifard, F., Jelinek, B., Peters, J. F. (2017). "Using DEM-LBM for Micro-Scale Modeling of Coupled Hydro-Mechanical Processes in Geomechanics". *Poromechanics VI: Proceedings of the Sixth Biot Conference on Poromechanics*, July 9-13, 2017, Paris, France, 238-245.

Lominé, F., Scholtès, L., Sibille, L., Poullain, P. (2013). "Modeling of fluid–solid interaction in granular media with coupled lattice Boltzmann/discrete element methods: application to piping erosion." *International Journal for Numerical and Analytical Methods in Geomechanics*, 37(6), 577–596.

Lu, N. (2016). "Generalized soil water retention equation for adsorption and capillarity." J. Geotech. Geoenviron. Eng., 10.1061/(ASCE)GT.1943-5606.0001524, 04016051

Lu, N., and Likos, W. J. (2004). Unsaturated Soil Mechanics, John Wiley & Sons, Inc., New York.

Martys, N. S., Chen H. D. (1996). "Simulation of multicomponent fluids in complex three-dimensional geometries by the lattice Boltzmann method." *Physical Review E*, 53(1), 743-750.

Noble, D. R. and Torczynski, J. R., (1998) A Lattice-Boltzmann Method for Partially Saturated Computational Cells. *International Journal of Modern Physics C*, 9: 1189–1201.

Owen, D. R. J., Leonardi, C. R., and Feng, Y. T., (2011) An efficient framework for fluid–structure interaction using the lattice Boltzmann method and immersed moving boundaries. *International Journal for Numerical Methods in Engineering*, 87 (1-5): 66–95.

Peters, J. F. and Walizer. L., (2013) "Patterned nonaffine motion in granular media." *Journal of Engineering Mechanics*, 139 (10): 1479–1490.

Peters, J. F., Kala, R., Maier, R. S., Walizer, L., Wibowo, J., Wahl, R. E., and Muthuswami, M., (2010) *User Guide for DEM*. U. S. Army Corps of Engineers ERDC, Vicksburg MS

Qian, Y. H., D'Humiéres, D., and Lallemand, P., (1992) "Lattice BGK Models for Navier-Stokes Equation." *EPL (Europhysics Letters)*, 17 (6): 479.

Rothman, D. H. and Zaleski, S., (2004) *Lattice-Gas Cellular Automata: Simple Models of Complex Hydrodynamics*. Aléa-Saclay. Cambridge University Press

Schaap, M. G., Porter, M. L., Christensen, B. S., Wildenschild, D., (2007). "Comparison of pressure-saturation characteristics derived from computed tomography and lattice Boltzmann simulations." *Water Resources Research*, 43(12), W12S06.

Shan X, Chen H. (1993). "Lattice Boltzmann model for simulating flows with multiple phases and components." *Physical Review E*, 47(3), 1815–1819.

Shan, X., and Chen, H. (1994). "Simulations of nonideal gases and liquid-gas phase transitions by the lattice Boltzmann equation", *Physical Review E*, 49, 2941-2948.

Strack, O. E. and Cook, B. K. (2007) "Three-dimensional immersed boundary conditions for moving solids in the lattice-Boltzmann method." *International Journal for Numerical Methods in Fluids*, 55 (2): 103–125.

Succi, S., (2001) *The lattice Boltzmann equation for fluid dynamics and beyond*. Oxford University Press, New York Sukop, M. C. and Thorne, D. T., (2006) Lattice Boltzmann Modeling - An Introduction for Geoscientists and Engineers. Springer, Berlin.

Sun, W., Kuhn, M. R., Rudnicki, J. W. (2013). "A multiscale DEM-LBM analysis on permeability evolutions inside a dilatant shear band." *Acta Geotechnica*, 8(5), 465–480.

Wolf-Gladrow, D. A., (2000) *Lattice-Gas Cellular Automata and Lattice Boltzmann Models: An Introduction*. Lecture Notes in Mathematics. Springer.